Available online at www.sciencedirect.com
ScienceDirect
Continental Shelf Research 28 (2008) 991–1009
CONTINENTAL SHELF RESEARCH
www.elsevier.com/locate/csr

Rapid formation of hyperpycnal sediment gravity currents offshore of a semi-arid California river

Jonathan A. Warrick*, Jingping Xu, Marlene A. Noble, Homa J. Lee

US Geological Survey, Coastal and Marine Geology Program, 400 Natural Bridges Road, Santa Cruz, CA 95060, USA

Received 30 August 2007; received in revised form 26 October 2007; accepted 5 November 2007
Available online 13 November 2007

Abstract

Observations of sediment dispersal from the Santa Clara River of southern California during two moderately sized river discharge events suggest that river sediment rapidly formed a negatively buoyant (hyperpycnal) bottom plume along the seabed within hours of peak discharge. An array of acoustic and optical sensors were placed at three stations 1 km from the Santa Clara River mouth in 10-m water depth during January–February 2004. These combined observations suggest that fluid mud concentrations of suspended sediment (>10 g/l) and across-shore gravity currents ($\sim$5 cm/s) were observed in the lower 20–40 cm of the water column 4–6 h after discharge events. Gravity currents were wave dominated, rather than auto-suspending, and appeared to consist of silt-to-clay sized sediment from the river. Sediment mass balances suggest that 25–50% of the discharged river sediment was transported by these hyperpycnal currents. Sediment settling purely by flocs ($\sim$1 mm/s) cannot explain the formation of the observed hyperpycnal plumes, therefore we suggest that some enhanced sediment settling from mixing, convective instabilities, or diverging plumes occurred that would explain the formation of the gravity currents. These combined results provide field evidence that high suspended-sediment concentrations from rivers (>1 g/l) may rapidly form hyperpycnal sediment gravity currents immediately offshore of river mouths, and these pathways can explain a significant portion of the river-margin sediment budget. The fate of this sediment will be strongly influenced by bathymetry, whereas the fate of the remaining sediment will be much more influenced by ocean currents.
Published by Elsevier Ltd.

Keywords: Hyperpycnal plume; Sediment; River mouth; Santa Clara River

1. Introduction

Rivers provide the largest source of sediment to the world's oceans, and transfer and dispersal of this sediment and associated materials influence sediment budgets of littoral, shelf, slope, and basin systems (Milliman and Syvitski, 1992; Syvitski et al., 2005), coastal primary productivity (Hutchins et al., 1998; Johnson et al., 1999), carbon sequesteration (Berner, 1982; Hedges and Keil, 1995; Gordon and Goñi, 2004), and fate and impact of pollutants and pathogens (Dojiri et al., 2003; Ahn et al., 2005). Large fluxes of sediment originate from the steep, short river basins of the world, and these rivers combine to produce more sediment output than the largest rivers of the world (Milliman and Syvitski, 1992).

A number of processes can dictate sediment dispersal pathways in coastal settings, including buoyant (hypopycnal) fresh water plumes, dilute suspended transport, negatively buoyant (hyperpycnal) sediment gravity currents, and the waves, currents and shelf morphology that influence these transport pathways (Wright and Nittrouer, 1995; Kineke et al., 1996; Geyer et al., 2000; Traykovski et al., 2000; Wright et al., 2001; Wright and Friedrichs, 2006). Recent advances in observation and modeling techniques have been used to identify hyperpycnal gravity currents as an important across-shore transport mechanism and a dominant supply of mud belt sediment (Trowbridge and Kineke, 1994; Wright et al., 2001, 2002; Scully et al., 2003; Harris et al., 2005; Traykovski et al., 2007). However, even with these advances it has been difficult to track the majority of river sediment dispersal, either owing to an underestimation of dilute suspended sediment transport or to processes or patterns not yet observed (Harris et al., 2005; Hill et al., 2007).

*Corresponding author. Tel.: +1 831 427 4793.
E-mail address: jwarrick@usgs.gov (J.A. Warrick).

0278-4343/$ - see front matter Published by Elsevier Ltd.
doi:10.1016/j.csr.2007.11.002

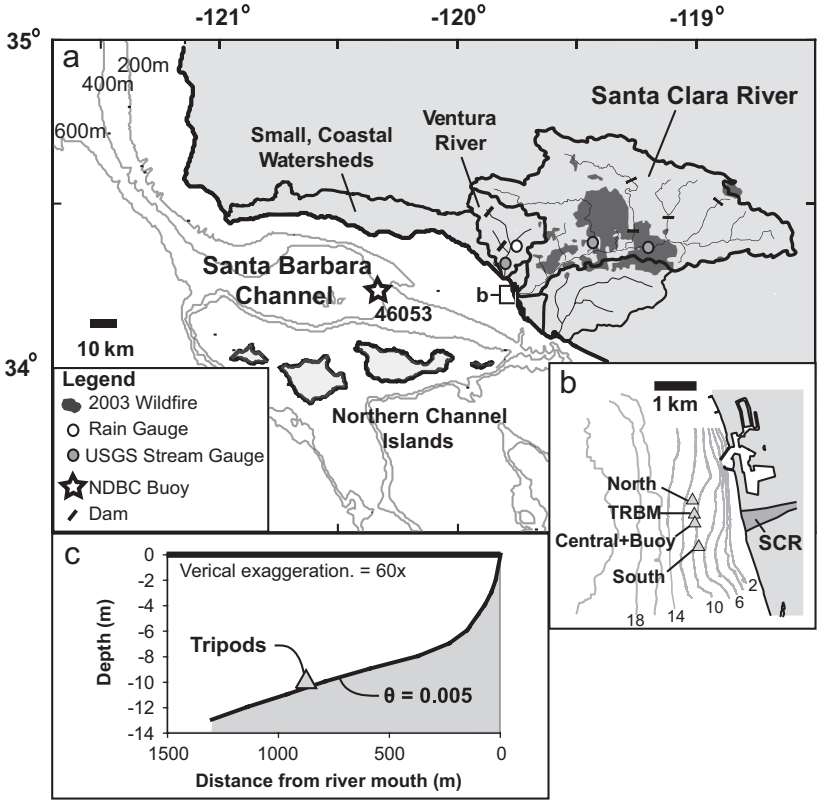

Fig. 1. (a) Map of the Santa Clara River watershed and Santa Barbara Channel region. (b) Inset map of the Santa Clara River (SCR) mouth region and bathymetry (in m) from RTK DGPS-echo sounder surveys with instrument locations during winter 2004. (c) Mean cross-shore profile from river mouth to moorings showing slope θ at the instrument sites of 0.005.

One hypothesized pathway for sediment dispersal is rapid settling immediately seaward of the river mouth. This may occur either from direct negative buoyancy of the river discharge from suspended-sediment concentrations in excess of ~40 g/l (Mulder and Syvitski, 1995; Warrick and Milliman, 2003) or from enhanced settling processes that would increase effective settling velocities far above individual or floc rates (Parsons et al., 2001, 2007; McCool and Parsons, 2004; Hill et al., 2007). Although there is a growing literature that shows that floc formation and the associated settling velocities are critical processes in river sediment dispersal (e.g., Hill et al., 2000; Wolanski et al., 2003; Milligan et al., 2007, George et al., 2007), there is little field evidence for either the rapid settling mechanisms suggested by Parsons et al. (2001) and McCool and Parsons (2004) or directly plunging the hyperpycnal river discharge.

In this study we investigated sediment transport immediately offshore of a small, mountainous river to evaluate dispersal processes during high sediment load and concentration events. The goal of this work was to evaluate the processes, timing, and importance of sediment transport along the seabed immediately offshore (~1 km) of the river mouth. The Santa Clara River of southern California (Fig. 1(a)) is a good site to study these processes, because it has been recognized to consistently produce high suspended-sediment concentrations (1–100 g/l) during winter discharge events (Fig. 2; Warrick and Milliman, 2003). Observations of the Santa Clara River hypopycnal plume suggest that over 90% of the suspended-sediment flux settles from this plume within 1 km of the river mouth (Mertes and Warrick, 2001; Warrick et al., 2004a). The results presented here provide new insights into the timing and processes of sediment plumes formed from a high-sediment yield river and provide evidence of rapid sediment settling processes and hyperpycnal sediment transport

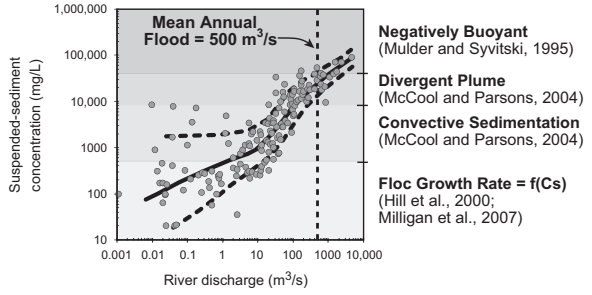

Fig. 2. Measured suspended-sediment concentrations for the Santa Clara River at Montalvo (USGS 11114000). Data have been fit with a local-weighted scatter smoothing (LOWESS) function (solid line), which is shown with one standard error (dashed line; *after* Warrick et al., 2004a. Also shown are oceanographic processes related to suspended-sediment concentration (shaded regions; see text) and the 2.3-yr recurrence annual peak discharge (mean annual flood, dashed vertical line).

immediately offshore of the river following river discharge events.

2. Data

2.1. Instrumented stations

A series of instrumented stations were deployed directly offshore of the Santa Clara River mouth with the primary objective of characterizing sediment transport along the seabed offshore of the river. The stations were placed ~1-km offshore of the river mouth along the 10-m isobath (Fig. 1(b)) and were deployed on January 22, 2004 to monitor 2004 winter storms. Stations included three benthic tripods with optical and acoustic sensors, a trawl-resistant bottom mount (TRBM) with a 1200 kHz RDI acoustic Doppler current profiler (ADCP), and a surface buoy with conductivity and temperature (CT) sensors (Figs. 1 and 3, Table 1). An alongshore distribution of stations was chosen because it was not known which direction the river plume would travel, and because it would allow for observations of radial dispersal, if it occurred.

The Central tripod was placed immediately seaward of the river mouth and was instrumented with a majority of the sensors. To estimate sediment concentrations at this tripod, one D&A Instruments type-3 optical backscatter sensor (OBS) was placed at 47 cm above the bed (cmab),

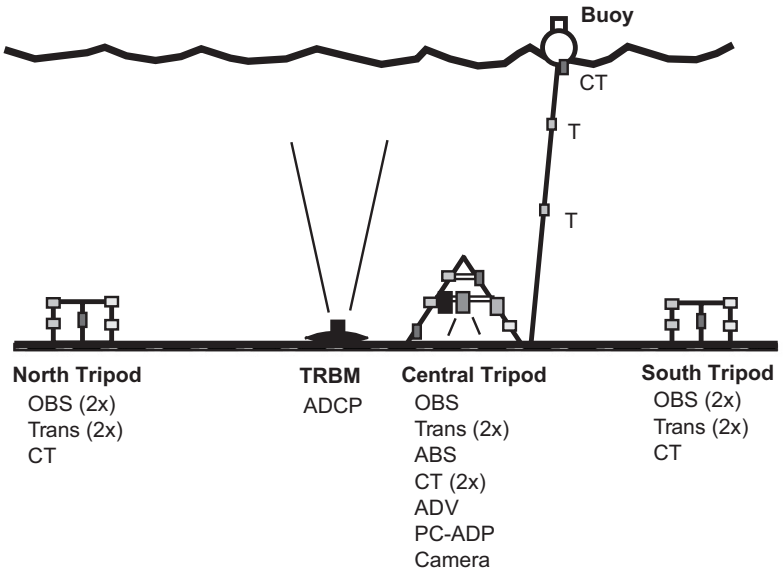

Fig. 3. Diagrams of the river mouth stations placed offshore of the Santa Clara River mouth. See Table 1 for details of instrumentation and sampling rates.

Table 1
Sampling information for the Santa Clara River mouth stations

Mooring	Instrument	Height (cmab)	Sampling
Central tripod	PC-ADP	104	1 Hz for 300 s every 15 min
	OBS	47	Burst sampled with PC-ADP
	Trans-10 cm	107	Burst sampled with PC-ADP
	CT	177	Burst sampled with PC-ADP
	Paros pressure	139	Burst sampled with PC-ADP
	ADV	75	1 Hz for 300 s every 30 min
	Trans-25 cm	189	Burst sampled with ADV
	ABS	94	2 Hz for 1200 s every 60 min
	CT	30	Sampled every 30 s
	Digital still camera	106	Sampled every 2 h
North and south tripods	CT	55	Sampled every 30 s
	OBS	47 and 105	Sampled every 30 s
	Trans	47 and 104	Sampled every 30 s
Surface buoy	CT	100 cmbs	Sampled every 30 s
	T1	400 cmbs	Sampled every 20 s
	T2	600 cmbs	Sampled every 20 s
TRBM	1200 kHz ADCP		Current burst: 5 min every 10 min Wave burst: 20 min every 2 h

and WET Labs transmissometers (Trans) with 10- and 25-cm path lengths were placed at 107 and 189 cmab, respectively. Depth-dependent suspended sediment patterns were evaluated with a three-frequency Aquatec AQUAscat acoustic backscatter sensor (ABS) placed at 94 cmab that sampled in 1 cm bins from 15 to 100 cm from the instrument. Water velocity was measured at the Central tripod with a Sontek acoustic Doppler velocimeter (ADV) that was placed 75 cmab and sampled at ~57 cmab and a Sontek pulse-coherent acoustic Doppler profiler (PCADP) looking downward from 104 cmab sampling at ~10 cm bins from approximately 10–80 cmab. Lastly, two SBE MicroCAT CTs were placed at 30 and 177 cmab, the lower CT was pumped, the upper was not. The North and South tripod stations were identical to each other, with OBS and 25-cm pathlength Trans at 47 and 105 cmab and pumped SBE SeaCAT CTs at 100 cmab. Details of the sampling frequencies of each sensor is shown in Table 1.

A camera system was placed on the Central tripod to characterize bedform evolution during the deployment; however, we also use these data to characterize the presence and characteristics of suspended sediment. A Canon EOS D60 digital SLR camera with 6-megapixel resolution was placed in a waterproof housing and mounted at 106 cmab. Photographs were taken every 2 h with lighting provided by a Deepsea strobe and scale provided with parallel red laser beams spaced 10 cm apart. Camera settings were fixed at (1/60) s shutter speed and an F-stop of f2.8. For each photograph we recorded whether the seabed was visible or not and mean output values for the three sensors (red, green, and blue), which were recorded in 8-bit output (i.e., 0–255).

A grab sample of the seabed sediment was obtained adjacent to the micropod site during deployment and had a median grain size d_{50} of 130 μm (well-sorted fine sand) as determined by sieving. One sediment trap was included on the Central tripod to collect suspended sediment for an evaluation of whether the grain size differed between suspended and local bed sediment. However, the sediment collected during the deployment was lost when the tripod toppled and later was recovered (discussed below). Thus, conversion of the ABS, OBS, and Trans data into sediment concentrations was only approximated due to the uncertainty in actual grain-size distributions during events. For much of this paper we present the OBS results in volts—medium gain settings were used for all OBS—and the Trans results as beam-attenuation coefficient (beam-c in m^{-1}). Beam-c was computed by manufacturer's recommendations using a calibration from the day of deployment, and approximate detection limits were 30 and 12 m^{-1} for the 10- and 25-cm transmissometer path lengths, respectively. We have used a similar technique as Sherwood et al. (2006) to present the ABS data, burst-mean profiles normalized by an empirical response profile that, for each frequency, is the binwise standard deviation from the median profile response. The ABS and OBS data are also compared using the techniques of Lynch et al. (1994) to approximate grain-size trends in the suspended sediment. We emphasize here that all sediment concentrations reported herein should be understood only as estimates because: (a) the actual grain-size distribution and floc fractions of the river sediment events—both of which have large and complex effects on optical and acoustic sensors (e.g., Ludwig and Hanes, 1990; Conner and DeVisser, 1992; Gibbs and Wolanski, 1992; Traykovski et al., 2000)—were not sampled, and (b) the maximum ranges of the Trans, ABS, and OBS were surpassed during the peak of sediment transport.

The stations became dysfunctional during February 26, 2004 due to a large wave event that toppled and/or buried each of the four benthic stations and dragged the buoy onto the beach. Fortunately, all the instruments were recovered by 6 days of diving operations. Although the cause, timing, and processes of mooring burial is of interest, we will not examine it here and focus rather on the sediment transport processes during the river discharge events.

2.2. Ancillary data

Hydrologic and meteorologic conditions were characterized by USGS and NOAA stations located within the region (Fig. 1(a)). Unfortunately, the historic USGS Santa Clara River mouth gauge (USGS 11114000—Santa Clara River at Montalvo), for which the sediment rating curve was developed (Fig. 2), was not operational during 2004, so other regional river gauges were used to evaluate river discharge. These included two within the Santa Clara River watershed (USGS 1113000—Sespe Creek near Fillmore; USGS 11109000—Santa Clara River near Piru) and one in an adjacent watershed (USGS 11118500—Ventura River near Ventura). Comparisons of these sites with the historic Santa Clara River mouth gauge (USGS 11114000) reveal that on average, discharge in the Sespe, Santa Clara near Piru, and Ventura Rivers were 36%, 41%, and 16%, respectively, of the historic discharge at the river mouth (data tabulated in Chapter 2 of Warrick, 2002). These rates were used to estimate discharge at the river mouth during the 2004 events.

Sediment discharge from the Santa Clara River was estimated using the discharge calculations and the suspended-sediment rating curve for the USGS 11114000 gauge complied in Warrick et al. (2004a) and shown in Fig. 2. For each 15-min estimate of discharge, sediment discharge was calculated by the product of river discharge and a discharge-dependent suspended sediment concentration estimate from Fig. 2. However, we note that ~10% of the Santa Clara River watershed was burned during fall 2003 (Fig. 1(a)), which may have increased sediment production in the watershed considerably. Assuming a 10-fold increase in erosion from the burnt area (cf. LACFCD, 1959; Taylor, 1981; Rice, 1982; Florsheim et al., 1991; Cerda, 1998; Lave and Burbank, 2004; Warrick and Rubin, 2007), the 2004 winter sediment discharge may

have been approximately 2-fold greater than the amount that would have been predicted from the historical rating curve.

Meteorologic (wind speed and direction, atmospheric pressure) and oceanographic conditions (wave height, period, and direction) were characterized with the NOAA NDBC buoy 40653 (Eastern Santa Barbara Channel; Fig. 1(a)). Precipitation data were obtained from the California Department of Water Resources—Division of Flood Management records for the OJA station in Ojai (Fig. 1(a)), which is the nearest hourly recording rain gauge and is operated by Ventura County (California Department of Water Resources (CADWR), 2007). Lastly, two satellite images of the Santa Barbara Channel were obtained from the NASA moderate resolution imaging spectroradiometers (MODIS) on the Aqua and Terra satellites. MODIS images are presented as "true-color" representations of the multi-band data provided by each sensor to approximate the RGB observations of the human eye.

3. Results

3.1. General conditions-winter 2004

During the instrument deployments meteorological and oceanic conditions exhibited a number of winter events. Rainfall and river discharge during the instrument deployments occurred in a series of events, the two largest are labeled E1 and E2 (Fig. 4(a) and (b)). Wave heights were also elevated for multiple day periods of time, including the three labeled W1, W2, and W3 and especially during the E2 event (Fig. 4(d)).

These five winter storms were also associated with the passing of fronts of low pressure (Fig. 4(f)) that included strong winds (Fig. 4(b)). South east winds ("upcoast") generally coincided with the arrival of the low-pressure fronts, while the northwest winds ("downcoast") occurred following the front passage consistent with Warrick et al. (2007). Storms could also be associated with the arrival of longer period waves of 16–18 s (Fig. 4(e)). The peak significant wave height during E2 was measured to be 5.4 m—over twice as large as the remaining period—with a dominant wave period of 17 s. This significant wave height has been surpassed only twice (both 5.6 m) in the 1994–2005 wave records for NDBC buoy 46053. This wave event was therefore approximately a 2–5-yr recurrence event and only 4% smaller than the maximum observed wave height for the buoy.

The two largest river events (E1 and E2) are of particular interest and are the focus of much of this paper, because of the sediment transport phenomena observed concurrent to these events. During these events pulses of river discharge peaked on February 22 and 26, respectively (Fig. 4(b)). River discharge during the E2 storm was approximately 10-fold greater than during E1. Using the historical hydrologic relationships discussed above, three regional gauges were used to estimate the peak discharge at Santa Clara River of 50 and 730 m^3/s during E1 and E2, respectively (Table 2). This places the E1 storm as somewhat common with a 1.2-yr recurrence interval, while the peak discharge during E2 has a 3-yr recurrence interval (cf. Warrick and Milliman, 2003).

Using the suspended-sediment rating curve for the Santa Clara River mouth (Fig. 2), the estimated peak discharges of E1 and E2 would have suspended-sediment concentrations of ~4 and ~30 g/l and sediment loads of ~0.008 and ~0.53 Mt, respectively (Table 2). However, as noted above wildfire may have increased the sediment production ~ twofold within the Santa Clara River landscape, which would result in peak suspended sediment concentrations of ~8 and ~60 g/l and loads of ~0.016 and ~1.06 Mt, respectively. These concentrations were adequately high to induce either strong convective settling or direct hyperpycnal discharge during both events as suggested by McCool and Parsons (2004) and Mulder and Syvitski (1995) (Fig. 2).

Lastly, it is noted that wave events W2 and W3 had minor storm river discharge associated with them. This contrasts with W1 in which no storm precipitation or discharge occurred (Fig. 4).

3.2. Surface plume observations

Salinity measurements of the surface waters at the buoy revealed fresh water pulses resulting from the river discharge during W2, E1, and E2 (Fig. 5(b)). The largest and longest salinity anomalies occurred during E1 and E2 when salinity decreased from ~33.3 PSU to a minima of 26 and 18 PSU during E1 and E2, respectively (Fig. 5(b)). These peak salinity reductions were short-lived, however, and the event salinities were typically ~28 to ~30 PSU during most of E1 and E2. As noted for the near-bed measurements below, these salinity observations may have been influenced by the suspended-sediment concentrations of the plume (high concentrations cause reduced conductivity and hence salinity). Although we do not have independent measurements of surface water sediment concentrations during E1 or E2, we note that previous sampling of the surface waters during similar events resulted in concentrations far too low (i.e., ~100 mg/l) to alter conductivity sensors (Mertes and Warrick, 2001; Warrick et al., 2004a). Assuming that the surface water salinity was solely caused by river freshwater with 0 PSU, the average event salinities suggest that the plume was only 10–16% river water, while 22% and 46% river water during peak salinity reductions.

Temperature at the buoy was generally independent of salinity during the freshened plume (Fig. 5(c)). This does not, unfortunately, allow for an independent identification of river water using temperature or T–S relationships, such as those possible for other plumes like the Columbia River (e.g., Nash and Moum, 2005).

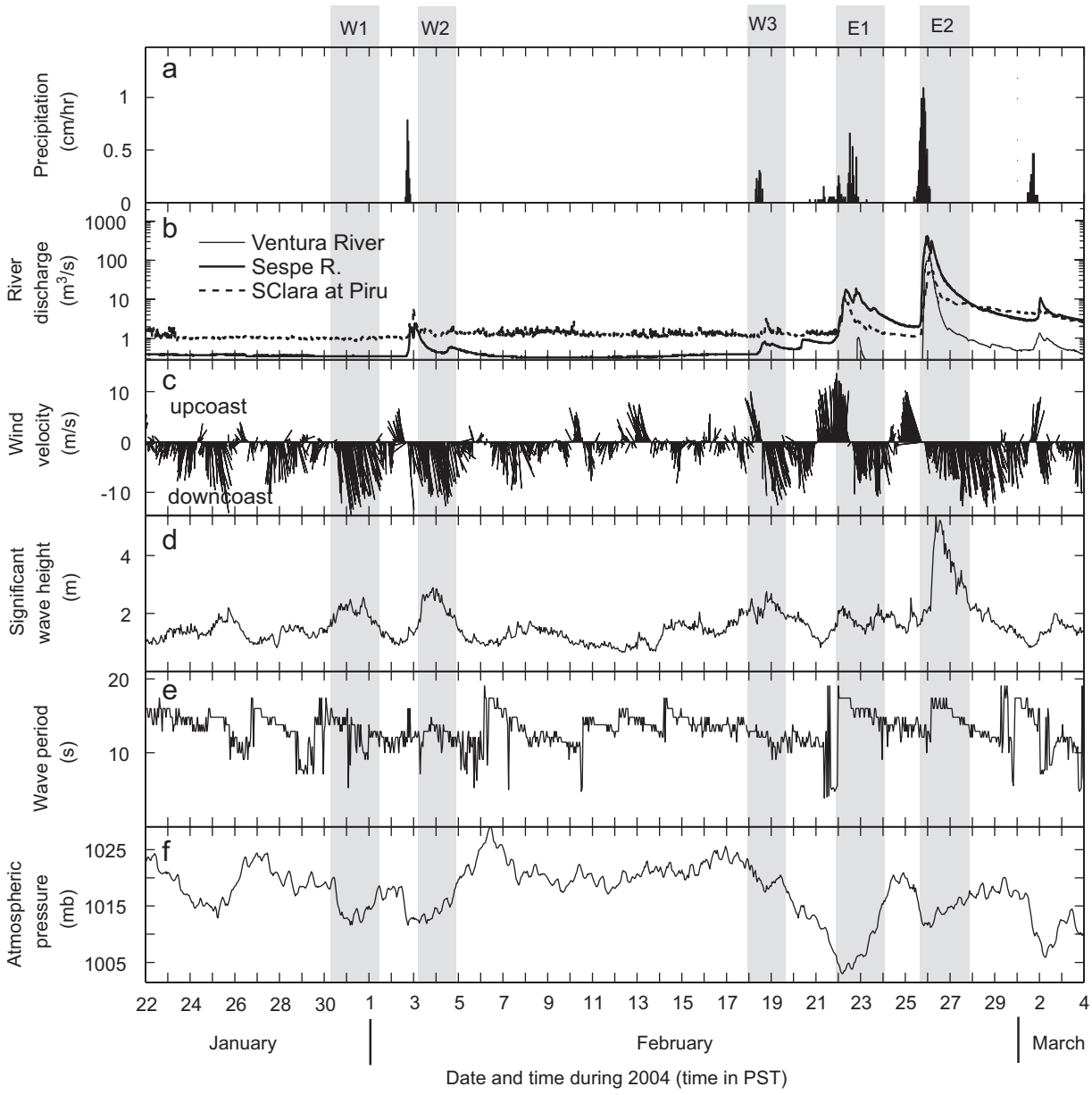

Fig. 4. General meteorological and oceanographic conditions during the winter 2004 instrument deployments. Shaded regions represent five events that are discussed in detail in the text and include both wave events (W1, W2, and W3) and river events (E1 and E2).

Reduced salinities at the surface buoy were only observed for ~20 h following both E1 and E2, and ambient salinity water (33.3 PSU) was observed following the fresh water pulses (Fig. 5(b)). The arrival and passing of the river water was marked by sharp changes in time, suggesting fronts in the salinity, a common characteristic along the boundaries of river plumes (e.g., Garvine, 1974).

Presence and movement of the surface plume was also observed in the satellite data (Fig. 6). The image obtained during E1 clearly reveals northwest (or "upcoast") movement of a turbid plume from the river mouth, which is consistent with the upcoast mean currents measured by the ADCP (Fig. 5(d)). In contrast, the plume during the image obtained during E2 has advected south of the river mouth (or "downcoast"; Fig. 6).

3.3. Bottom plume observations

3.3.1. Salinity and suspended sediment

The measurements obtained from the Central tripod (Fig. 7) suggest that there were clear signals of elevated suspended sediment in the Trans, OBS, and ABS data during the wave events (W1–W3) and the river events (E1 and E2). However, E1 and E2 were unique due to: (1) reduced salinity measurements on the order of 3–5 PSU (Fig. 7(b)); (2) elevated sediment concentrations, often near or in excess of the measurable range of the instruments (Fig. 7(c)–(f)); (3) water color that was exceptionally red (Fig. 7(e)); and (4) strong initial fronts in these parameters (Fig. 7(b)–(f)). Below we examine these conditions individually prior to incorporating them with other observations.

Table 2
Hydrologic and oceanographic conditions of the two largest storm events of the monitoring period

Event number	E1	E2
Date of peak discharge	February 22, 2004	February 26, 2004
Peak discharge of Santa Clara River[a]	50 m^3/s	730 m^3/s
Maximum river suspended-sediment Concentration		
From rating curve[b]	4 g/l	30 g/l
Including wildfire effects[c]	8 g/l	60 g/l
River suspended-sediment flux		
From rating curve[b]	0.008 Mt	0.53 Mt
Including wildfire effects[c]	0.016 Mt	1.06 Mt
Characteristic values of		
u_w	45 cm/s	45 cm/s[d]
T_{dom}	16–18 s	14–16 s[d]
v_c	5–10 cm/s	0–15 cm/s[d]
u_g	5 cm/s	5–10 cm/s[d]

[a]Estimated discharge for the river mouth gauging station USGS 11114000—Santa Clara River at Montalvo from the three regional river gauges (see text).
[b]Suspended sediment rating curve from Warrick et al. (2004).
[c]Wildfire effects assumed to double sediment production (see text).
[d]Estimated from the first portion of event E2 prior to an increase in wave height and observation failure.

Reduced salinity during the events may have been the result of either: (1) the injection of fresh river water to the seabed, or (2) fouling of the conductivity measurements by excessive concentrations of suspended sediment (e.g., Kineke et al., 1996; Traykovski et al., 2000). We first examine the potential for fresh water injection, which may have occurred by either: (a) downward mixing of the hypopycnal toward the seabed or (b) direct injection of fresh water along the seabed through river water–sediment mixtures. Downward mixing of the surface plume is not supported when the salinity observations at 30 and 177 cmab are compared, because the measurements at 177 cmab do not show similar decreases (Fig. 7(b)).

Direct fresh water injection along the seabed by a hyperpycnal plume may explain the salinity observations; however we note that this plume would require exceptional sediment concentrations (~10 g/l), which would confound the ability to observe such freshwater due to sediment fouling of the conductivity measurements. Although freshwater injection within a hyperpycnal plume cannot be ruled out, we note that this water does little to modify the salinity properties within ~1 m of the upper portion of this plume. On the contrary, if the reduced salinity measurements were caused entirely by excessive sediment concentrations, Traykovski et al. (2000) suggest that this effect can be assessed with Archie's Law:

$$\rho_{measured}/\rho_{seawater} = \phi^{-m}, \quad (1)$$

where ρ is the resistivity (conductivity^{-1}), ϕ the porosity of the sediment, and m is an empirical parameter between 1.2 and 3 (Archie, 1942; Jackson et al., 1978). Assuming that the conductivity fluctuations resulted entirely from high concentrations of sediment, the porosity ϕ of this water–sediment mixture is predicted to be 2.4–5.8%. This is analogous to suspended sediment concentrations of 63–160 g/l, well above the ~10 g/l threshold for fluid mud (Traykovski et al., 2000). If river water had also been incorporated into these water–sediment mixtures, the necessary sediment concentrations to produce these conductivity changes would be lower.

The salinity anomalies during E1 and E2 coincided with highly turbid conditions as shown by the OBS and Trans sensors (Fig. 7(c) and (d)). The beam-c measurements were consistently greater at 107 cmab than at 203 cmab, and the majority of the E1 and E2 observations at 107 cmab were in excess of the measurable limit of 30 m^{-1}. However, this maximum limit would be exceeded by suspended-sediment concentrations of only ~40 mg/l using the calibration data for fine sediment in the Santa Clara River surface plume of Warrick et al. (2004a). The OBS measurements similarly showed strong fronts during the event initiation, and the peak measured values reached the instrument limit of 5 V (Fig. 7(d)). For this OBS and a silt sediment grain size, these OBS values would correspond to suspended-sediment concentrations that were 1–10 g/l. Concentrations at the OBS may have been higher, because the burst-sampled OBS outputs may have surpassed the nonlinear output thresholds (cf. Kineke and Sternberg, 1992).

Photographs from the camera system also provide insights to the sediment transport events. The turbidity of the lower water column obscured the seabed during much of the deployment (Fig. 7(e)). Examples of these photographs are shown in Fig. 8 and noted in the time series of Fig. 7(e). These photos show that the orange-to-brown turbid colors during events E1 and E2 (Fig. 8(c), (e)) were quite different than the gray–tan colors during local resuspension events (Figs. 8(b) and (d)). These qualitative patterns were characterized with mean color output values of the photos, which tended to have lower green and blue and higher red values during E1 and E2 than at other times (e.g., Fig. 8). A time series of the ratio of red-to-green (R/G) reveals that the sediment suspended in photos taken during E1 and E2 were much redder than the remainder of the record (Fig. 7(e)).

The ABS results revealed that high backscatter associated with the seabed was not observed for ~6 h during E1 and E2, and that instead a lower backscatter layer was observed 10–20 cmab (Fig. 7(f)). A comparison of all three ABS wavelengths with the range to seabed results of the ADV and PCADP is provided in Fig. 9. An increase in elevation of the maximum backscatter was observed during E1 and E2 in both the 5 and 2.5 MHz data, and these observations coincide with the low salinity anomalies and seafloor range anomalies of ~15 cm from the ADV and PCADP (Fig. 9). Raw ABS data during E1 reveal how the acoustic return of the seafloor was initially lost and gradually returned over the coarse of many hours (Fig. 10).

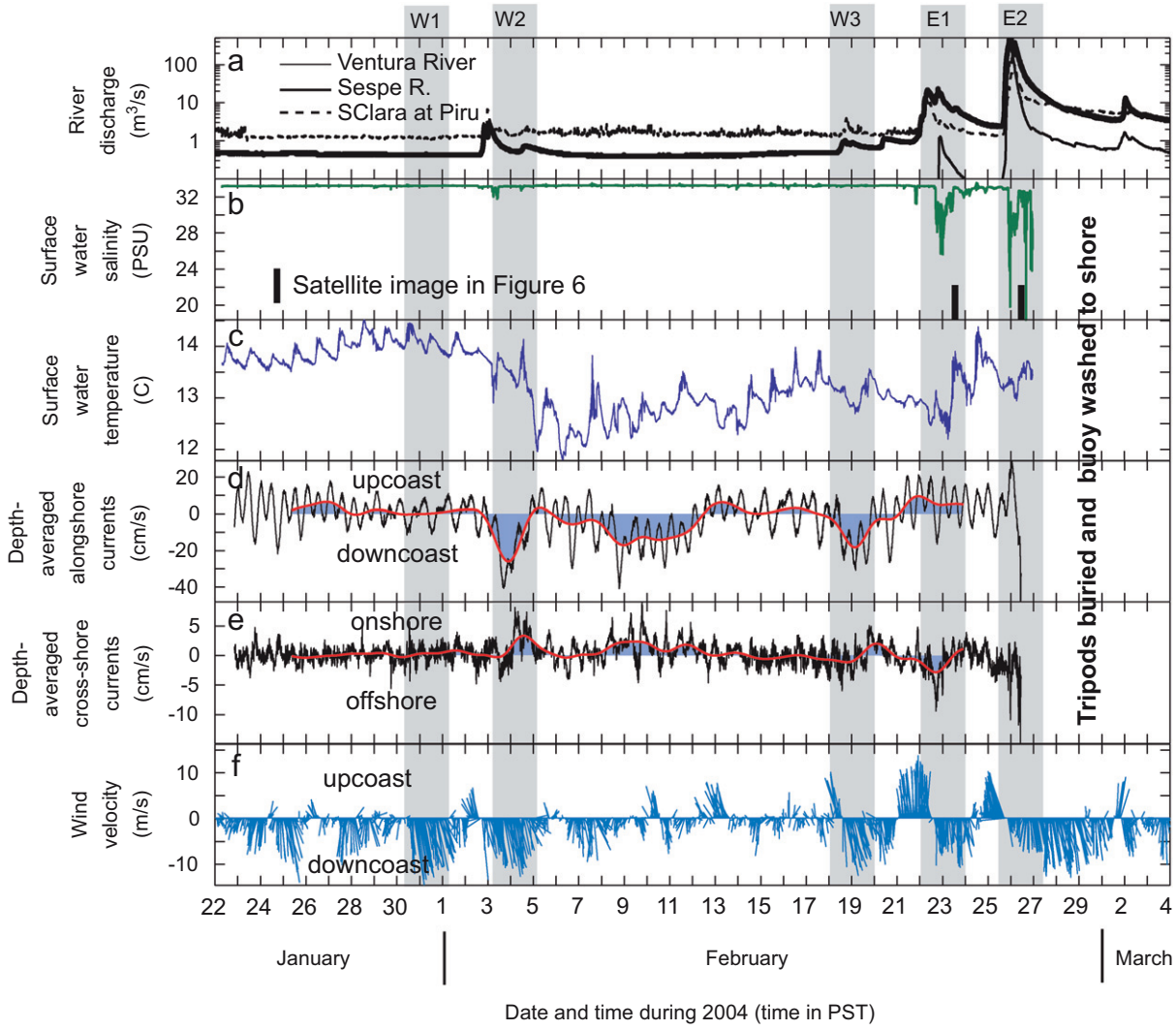

Fig. 5. Observations during the winter 2004 relevant to the buoyant plume of the Santa Clara River including (a) river discharge, (b) surface water salinity, (c) surface water temperature, (d, e) depth-averaged currents, and (f) alongshore winds. Shaded regions represent the five events that are discussed in detail in the text.

These ABS data suggest a sudden presence of a layer of sediment with a diffuse upper boundary and adequate sediment concentrations to attenuate the 5 and 2.5 MHz signals.

The ADV and PCADP acoustic range measurements are based on the presence of strong returns from an apparent surface, and the ability of each sensor to determine a seabed elevation was compromised during both E1 and E2. For example, the ADV had a 37% success rate for identifying the seabed range during the first half of E1, a 35% success rate during E2, but 88% success during the entire record. This suggests that during E1 and E2: (1) a layer of highly concentrated sediment was present that acoustically dampened the seabed for periods of hours and (2) a gradient in sediment concentration occurred near 10–20 cmab (Fig. 9).

Grain-size information can be obtained by comparing the 5 MHz ABS and the OBS data obtained at the same elevation (47 cmab). As shown by Lynch et al. (1994) the ratio of the ABS to OBS signals—if neither has nonlinear attenuation—is proportional to the mean grain-size diameter d. We compiled hourly averaged ABS and OBS data for each of the five events (Fig. 11) and assumed that the suspended sediment during W1 was solely from bed sediment ($d = 130\,\mu m$; cf. Fig. 4). The median ABS/OBS ratios for E1 and E2 were 20–30 times smaller than for W1 (Fig. 11), which suggests that d may have been 4–6 μm during E1 and E2. These analyses also suggest 3–4 fold reductions in the ABS/OBS ratio during W2 and W3 (i.e., $d = 30$–$45\,\mu m$; Fig. 11), which may be due to minor additions of fine sediment from river discharge (cf. Fig. 4). Although these calculations suggest a 20–30-fold reduction in d during E1 and E2, we note that they may be somewhat conservative due to the apparent nonlinear nature of the OBS during these events (Fig. 7).

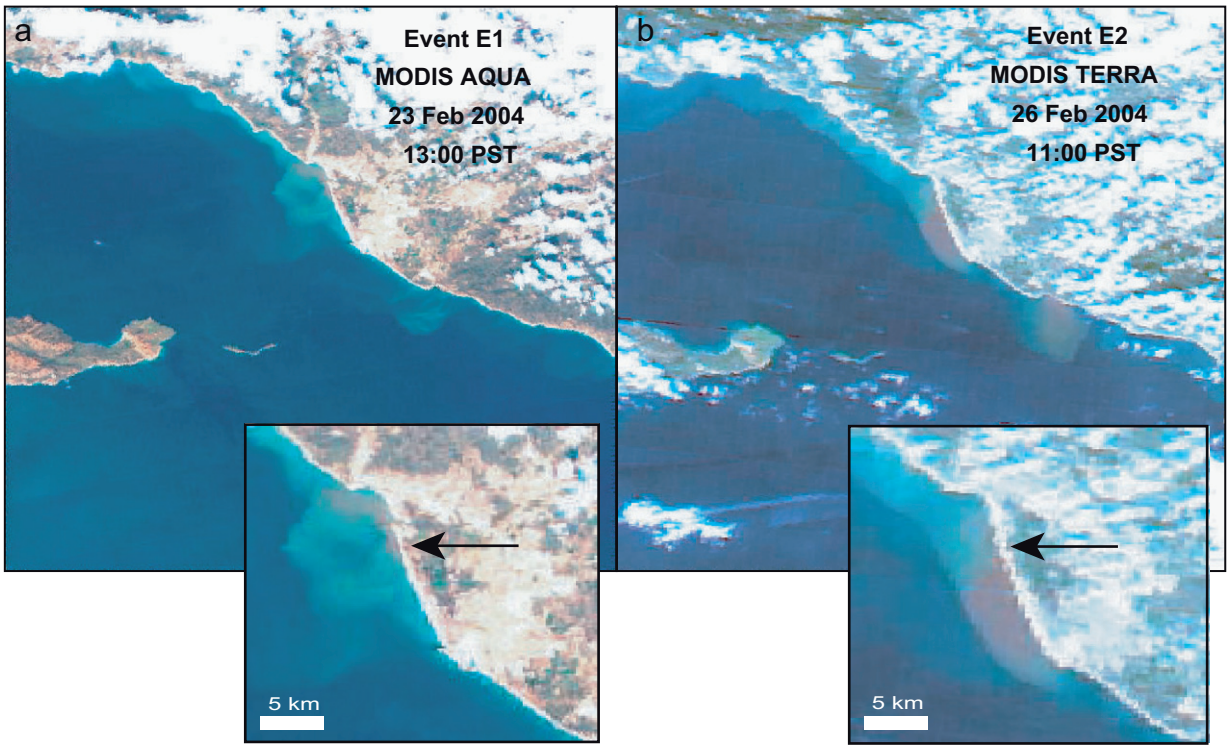

Fig. 6. True-color presentation of multi-spectral MODIS imagery obtained during the two river events E1 and E2. Insets show the river mouth region with the location of the Santa Clara River mouth identified with an arrow.

We note that the two sediment transport events, E1 and E2, were initiated without significant change in the wave orbital velocities (Fig. 12), whereas other wave events in the observations clearly caused sediment resuspension at the mooring sites (Fig. 7). It is highly unlikely then that events E1 and E2 were caused simply by resuspension of local sediment.

3.3.2. *Near-bed currents*

The near-bed currents show evidence for cross-shore transport concentrated along the seabed. Summaries of the mean cross-shore ADV and PCADP data are shown in Fig. 12. The mean cross-shore bottom currents measured by the ADV at 57 cmab and the PCADP at 60 cmab were generally quite similar, although the PCADP data were more variable in time (Fig. 12(b) and (f)). The PCADP current profiles reveal that cross-shore currents had near-bed intensification during E1 and E2. This is shown in Fig. 12 by greater cross-shore currents at 30 cmab than at 60 cmab during both E1 and E2. Hourly profiles of mean cross-shore currents during E1 are shown in Fig. 13, most having maximum offshore velocities in excess of 5 cm/s and centered at 20–40 cmab. Near-bed cross-shore current shear was even greater during E2 than E1 (Fig. 12). These cross-shore currents are highly indicative of a high-concentration sediment gravity currents in the bottom 20–40 cm of the water column as discussed by Traykovski et al. (2007).

3.3.3. *Burial of the ADCP*

The TRBM-ADCP data were used to characterize the vertical distribution of currents and suspended sediment and show a intriguing burial pattern. Acoustic scattering volume (ASV), which is a surrogate for suspended-sediment concentration derived from the ADCP data (e.g., Thorne et al., 1993), was calculated from the raw echo intensity using the techniques of Hoitink and Hoekstra (2005). These ASV data showed that elevated amounts of sediment were common along the seabed throughout the experiment and may have been associated with the E1 buoyant surface plume (Fig. 14). The E1 sediment transport event was observed by the Central tripod sensors (Fig. 14(d)) approximately 30 min before the ASV data, suggest that the remaining water column revealed elevated acoustic scattering (Fig. 14(b)). This may suggest that a lateral source of suspended sediment was the cause of the E1 event, rather than a ''top–down'' source directly from the surface plume. Approximately an hour after the initiation of E1, the ADCP signal strength and ASV dropped dramatically (Fig. 14). This reduced return at the height of sediment transport is likely due to acoustic attenuation from excessive suspended sediment or sedimentation on top of the instrument. The acoustic attenuation was ~50 dB across all ADCP bins (Fig. 14(c)). The depth of sediment that would induce this attenuation can be estimated from acoustic data from Hamilton (1972), which suggest that for 1200 kHz the

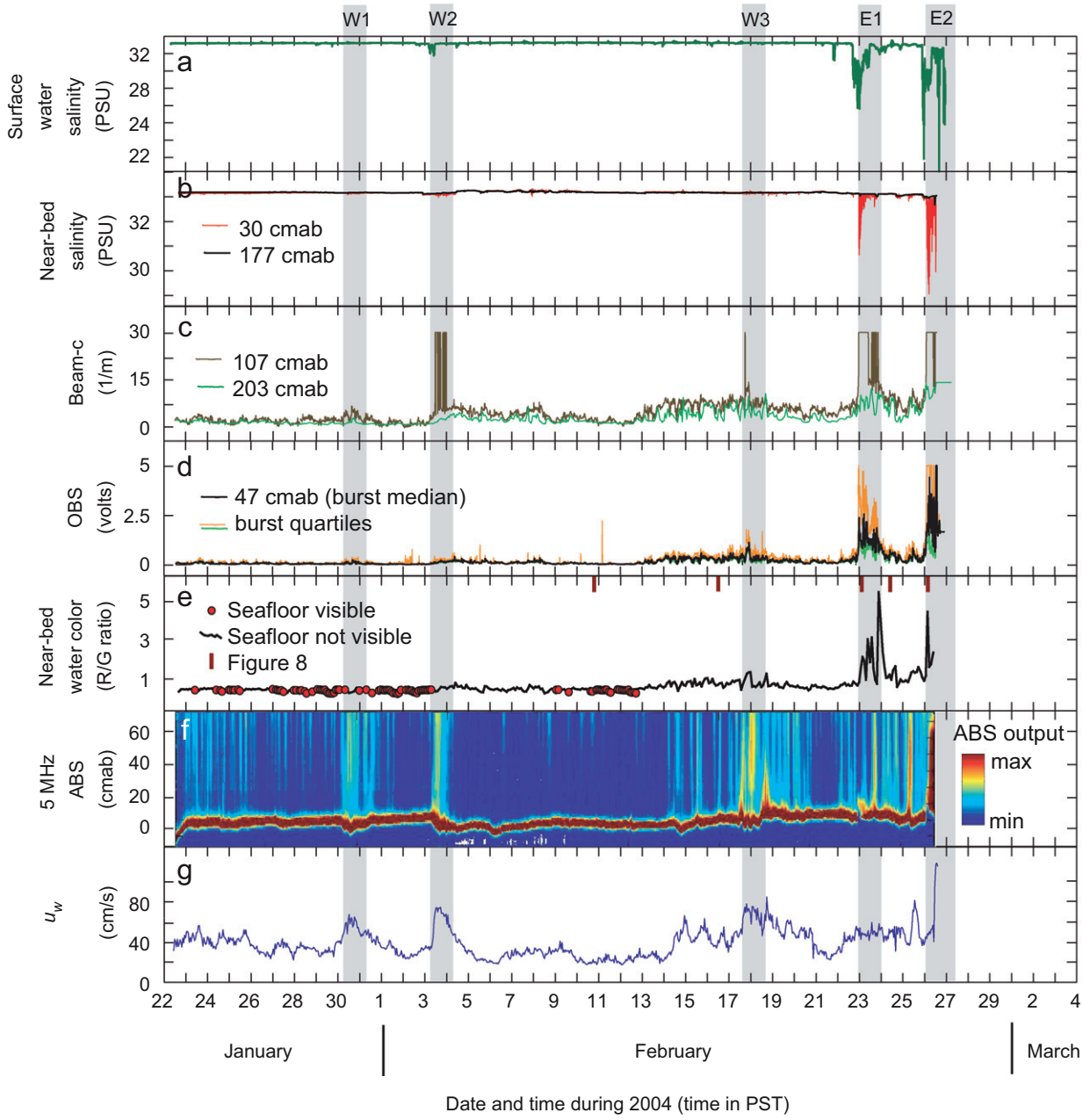

Fig. 7. Observations during the winter 2004 relevant to the near-bed conditions at the Central tripod and buoy, including (a) surface water salinity, (b) near-bed salinity, (c) beam attenuation, (d) optical backscatterance, (e) near-bed water color from the digital camera, (f) acoustic backscatterance, and (g) u_w ($=2^{0.5}u_{rms}$) from the ADV. Shaded regions represent the five events that are discussed in detail in the text.

attenuation should be 100–500 dB/m. Thus, the range of sediment thickness is estimated to be 10–50 cm, the low and high values associated with sand and mud, respectively. We note that these thicknesses are for sediment in natural marine settings and have porosities ranging 38–66%.

3.3.4. North and South tripods

The North and South tripod data were compared with the Central tripod data to evaluate the lateral extent of sediment dispersal. For E1 and E2, the OBS and Trans observations were consistently higher at the North and South tripods than at the Central tripod (data not shown). Further, all bottom moorings measured drops in salinity during the peak transport events, the magnitude of which was proportional to the height above the seabed (data not shown). A comparison of the timing of the bottom plume arrival suggests that the plume during both E1 and E2 arrived at the South tripod 20 min before the Central tripod, which in turn was 20 min before the North tripod. On the scale of 4–6 h dispersal timing, these differences are likely insignificant and may just be related to station distance from the river mouth (Fig. 1(b)) rather than lateral transport variability.

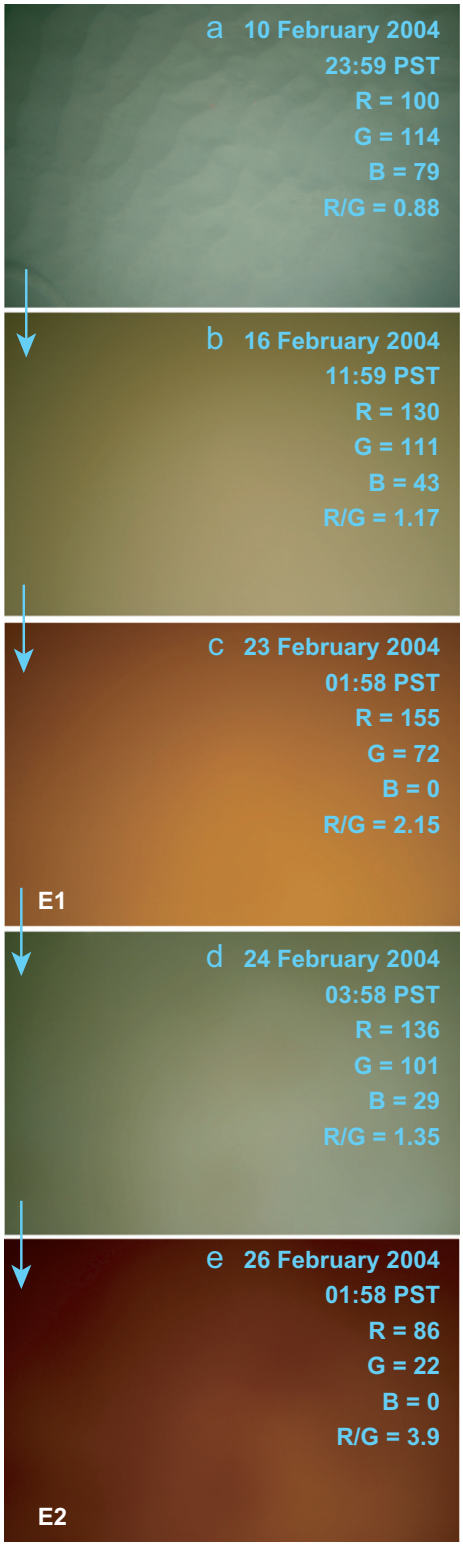

Fig. 8. Examples seabed digital photographs from the photographic time series taken from 106 cmab. Raw photograph statistics for the three color sensors (R, G, and B) and the R/G ratios are shown for each photo. Photos obtained during the two largests events are labeled with E1 and E2. A time series of the R/G ratio data is shown in Fig. 7(e).

4. Interpretations

4.1. Integration of observations

The combined observations suggest that unique sediment transport events occurred 4–6 h after the two largest river discharge events. The characteristics of these events included: (1) near-bed sediment concentrations in excess of several g/l and likely tens of g/l; (2) cross-shore currents that were directed offshore at rates of ~5 cm/s with the greatest speed at 20–40 cmab; (3) sediment colors that were red-brown; (4) a layer 10–20 cm thick that had an acoustically diffuse upper boundary and adequate sediment concentrations to attenuate the 2.5 and 5 MHz signals; (5) apparent suspended-sediment grain-size diameters 20–30 times smaller than the 130 μm bed sediment; (6) apparent burial of the shallowest station (TRBM); (7) sharp initial interfaces in all of these transport characteristics; and (8) no coincidental increase in wave orbital velocities.

Combined, these observations strongly suggest that fluid mud concentration sediment gravity currents occurred during the two events. Wright and Friedrichs (2006) and Traykovski et al. (2007) both note that similar wave-supported events are observed offshore of other small rivers such as the Po and Eel and hypothesize that these events may be an important sediment transport mechanism for many of the world's rivers. The events observed at the Po and Eel similarly occurred in layers O(10 cm) with sediment concentrations O(10 g/l) and near-bed cross-shore velocities O(10 cm/s). One conclusion of these researchers is that for gravity currents to occur, there must be adequate supply of fine-grained sediment and ample wave-orbital or current velocities. Below we show that our observations closely match sediment transport theory derived from the Po and Eel. However, we note that the Santa Clara River events occurred much closer to the river mouth than what the previous theory would suggest.

4.2. Application of theory

A first-order, wave-averaged model for hyperpycnal sediment gravity currents was presented by Wright et al. (2001) and shown to be generally applicable by Scully et al. (2003), Wright and Friedrichs (2006), and Traykovski et al. (2007). Using Chezy-type formulations, the Wright et al. (2001) model suggests that

$$B \sin\theta = C_D |u| u_g, \tag{2}$$

where B is the depth-integrated buoyancy anomaly (m^2/s^2) in the high suspended-sediment concentration layer, θ the bed slope, C_D the bottom drag coefficient ranging between 0.003 and 0.005, $|u|$ accounts for the combined influence of gravity-driven downslope velocity u_g, the amplitude of the wave-induced orbital velocity $u_w = 2^{0.5} u_{rms}$, and near-bed velocity v_c on the quadratic friction term and is defined to be $(u_g^2 + u_w^2 + v_c^2)^{0.5}$.

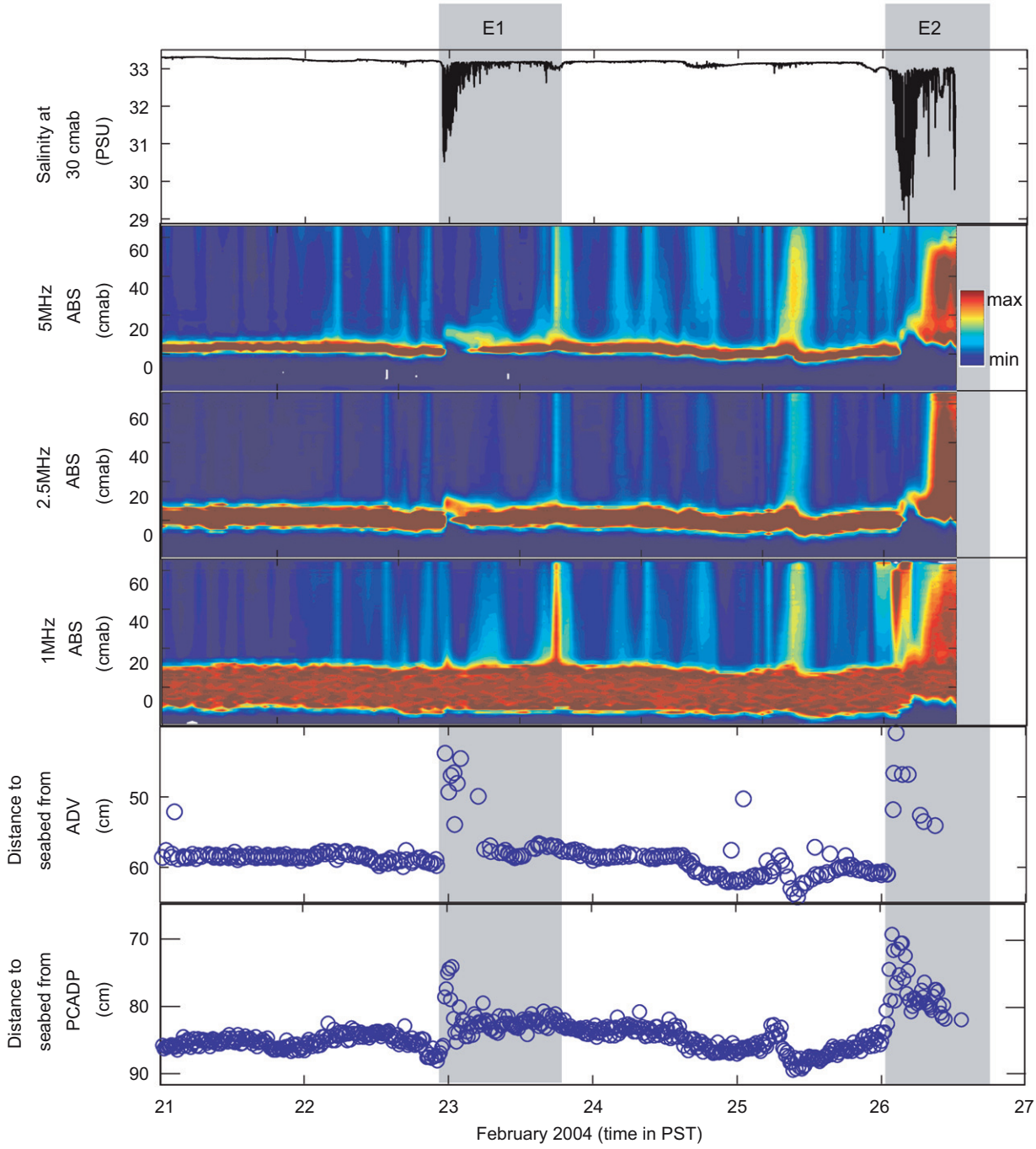

Fig. 9. Acoustic backscatterance from the ABS and estimates of the range to seabed from two acoustic sensors (ADV and PCADP) during the two river discharge events, E1 and E2 (shown with shading).

An important criterion is that resuspension-settling feedback develops that is related to turbulence suppression from the buoyancy anomaly and turbulence generation by shear in the boundary layer (Trowbridge and Kineke, 1994; Kineke et al., 1996). This effect results in the maintenance of a critical value on the order of 0.25 for the bulk Richardson number Ri of the flow, approximated to be $B|u|^2$. One ramification of this is that the minimum seabed slope in which self-maintenance occurs without influence from u_w or v_c is

$$\sin\theta = C_D/Ri_{cr}. \tag{3}$$

Hence, the minimum θ (in radiaus) for a self-maintaining fluid mud is 0.01–0.02 (cf. Wright and Friedrichs, 2006).

Applying this theory to the Santa Clara River observations, we note that the actual θ in the vicinity of the Santa Clara River, 0.005 radians (Fig. 1(c)), is significantly smaller than the self-maintaining threshold. Hence, we do

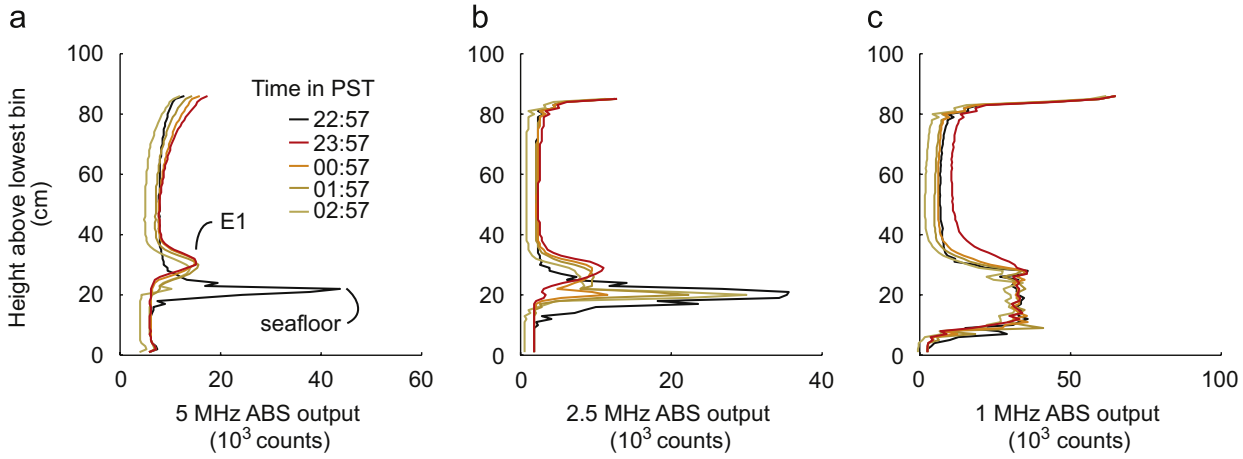

Fig. 10. Raw burst-averaged output from the ABS during event E1. The final pre-event profile is shown in black, and E1 profiles are shown with red-brown colors.

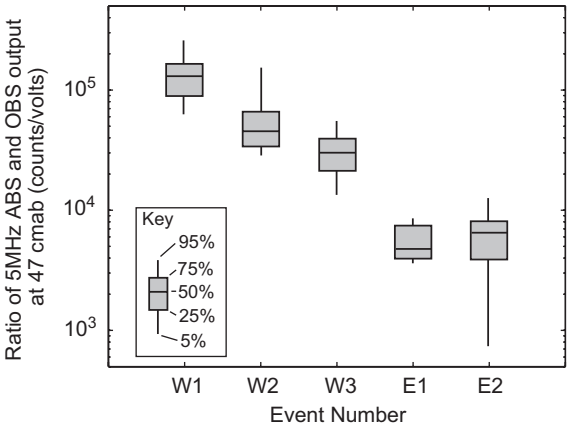

Fig. 11. Comparison of the output of the ABS and OBS sensors at the same depth during the five events. The ratio of the ABS and OBS may be related to suspended sediment grain size as suggested by Lynch et al. (1994).

not expect that the transport events observed offshore of the Santa Clara River were self-maintaining. However, u_w and v_c were ~45 and ~10 cm/s, respectively, during both events (Fig. 12; Table 2). Using u_g of 5 cm/s, $|u|$ is computed to be 46 cm/s, and the gravity currents are predicted to be "wave supported" due to the dominance of u_w in $|u|$.

The maximum sustainable suspended load with unlimited sediment supply would result in critical loads B_{cr} and gravity current velocities u_{gcr} of

$$B_{cr} = Ri_{cr}|u|^2 \tag{4a}$$

and

$$u_{gcr} = (\sin\theta)Ri_{cr}|u|/C_D. \tag{4b}$$

This would result in a B_{cr} of 0.053 m^2/s^2 and u_{gcr} of 12–19 cm/s for the events observed. We note that the observed u_g were less than half the predicted critical value during both events (Table 2), which suggests that the gravity currents were not at the maximum sustainable sediment load; and if provided more sediment, this sediment could have been incorporated into the hyperpycnal current. The actual buoyancy flux during both events can be estimated by

$$B = C_D|u|u_g/\sin\theta \tag{5}$$

to be 0.014–0.023 m^2/s^2, or roughly a third to half of the maximum flux. This buoyancy anomaly would be equivalent to the following depth-averaged layer:

$$B = gsC'h, \tag{6}$$

where g is the gravitational constant (9.81 m/s^2), s the submerged specific gravity of sediment (~1.6), C' the depth-averaged sediment concentration, and h the thickness of the flow. From the combined observations presented above (Figs. 9, 10, 12 and 13), we suggest that h was 15–40 cm. Rearranging Eq. (6), we predict that the time- and depth-averaged volumetric suspended-sediment concentration C' was ~0.006 (predicted range = 0.002–0.010), which corresponds to a mass concentration C'_s of ~16 g/l (range = 5–26 g/l) assuming a sediment density of 2600 kg/m^3. These predictions are consistent with our combined observations of suspended sediment and with the conclusion that the events were dominated by fluid mud conditions (i.e., greater than or equal to ~10 g/l).

Traykovski et al. (2000; 2007) have observed that the thickness of sediment gravity currents (or the "lutocline height," δ_w) under wave-dominated conditions could be predicted accurately with the wave boundary layer thickness based on the wave friction factor f_w:

$$\delta_w = (f_w/8)^{0.5}u_w/\omega_r, \tag{7a}$$

$$f_w = 0.04(u_{bsig}/\omega_r k_n)^{-0.025}, \tag{7b}$$

where ω_r is the radian wave frequency, u_{bsig} the significant wave velocity equivalent to $2u_{rms}$, and k_n the roughness scale equivalent to $30z_0$, where z_0 is the bed roughness (cf. Smith and Mclean, 1977; Wiberg and Smith, 1983;

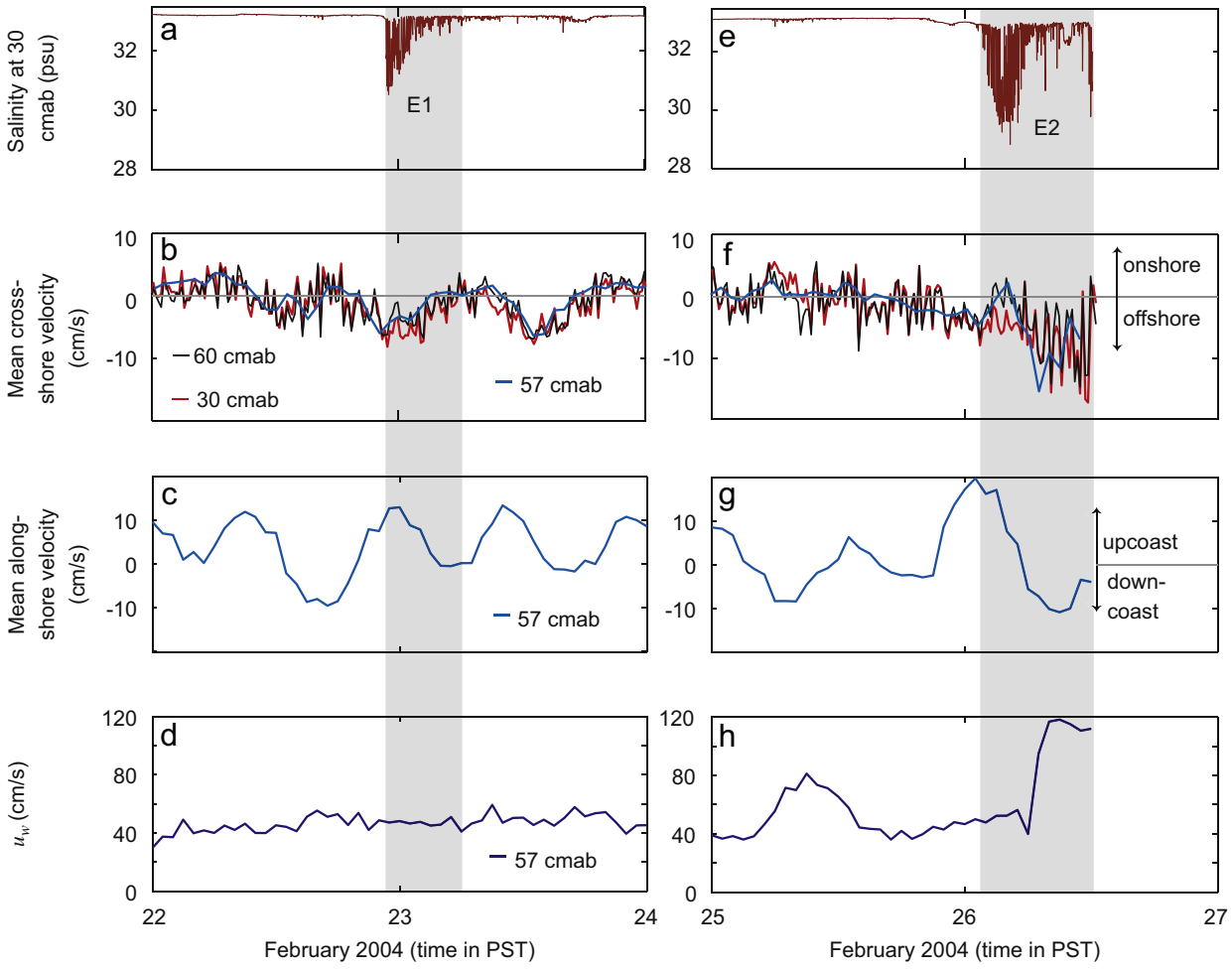

Fig. 12. Near-bed velocity observations from the PC-ADP and ADV during event E1 (a)–(d) and E2 (e)–(h). Burst-averaged cross-shore velocities are shown for 30 and 60 cm above bed (cmab) for the PCADP and 57 cmab for the ADV. Mean alongshore and wave orbital velocities (u_w) are calculated from the ADV observations. (a) and (e) Salinity at 30 cmab (psu); (b) Mean cross-shore velocity (cm/s) and (f); (c) and (g) Mean alongshore velocity (cm/s) and (d) u_w (cm/s).

Fredsøe and Deigaard, 1992). We used a z_0 range of 0.01–1 cm, which would represent flat to rippled seabed conditions, and estimated δ_w to be ~8 cm during E1 and the first half of E2. Estimates of the lutocline height from the inflection of the velocity profiles (Fig. 13) and acoustic sensors (Fig. 10) range 15–40 cm. The significantly higher lutocline height observations may be the result of wave-generated vortices exchanging mass and momentum above the predicted wave boundary layer. Lee et al. (2002), for example, observed the wave boundary layer thickness to grow to 30 cm over fine sand at 13-m depth off Duck, NC, during times when long-period waves coincided with weak along-shore currents.

4.3. Sediment mass balance

A mass balance of sediment can be developed using the observations and theory presented above. We note that all of the sediment sensors were likely above the hyperpycnal layer for both events, and hence we utilize the current measurements to estimate a flux time series. Using the concepts presented above, a mass balance of sediment flux Q_s for the E1 event can be computed by

$$Q_s = whu_g C'_s, \tag{8}$$

where w is the width of the current, which was conservatively estimated to be 1600 m, the total distance between the three moorings. Hourly estimates of h (0-40 cm), u_g (0–6 cm/s), and $|u|$ (45–50 cm/s) were obtained from the PCADP and ADV observations, and these data were combined to compute B, C', and Q_s for the E1 event. Hourly flux estimates revealed a sharp initial front—consistent with other measurements—and resulted in ~4.2 kt of sediment transported during E1 (Fig. 15). This is equivalent to ~25–50% of the estimated river load (cf. Table 2). We note that the flux estimate may be conservative, because it assumes minimal radial spreading of the plume from the river mouth and no transport above the gravity current. However the uncertainty of this estimate is at least 50%. Regardless, a substantial portion

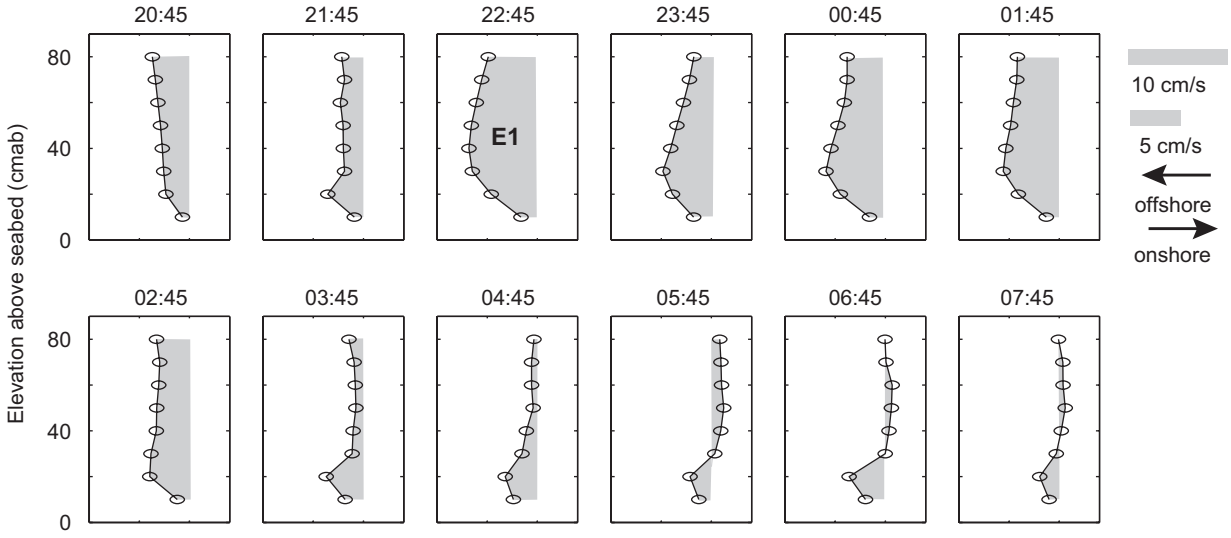

Fig. 13. Time series of nearbed mean hourly across-shore current profiles from the PCADP during the sediment transport event E1. The initiation of the transport event is labeled as "E1." Shading is provided from zero velocity.

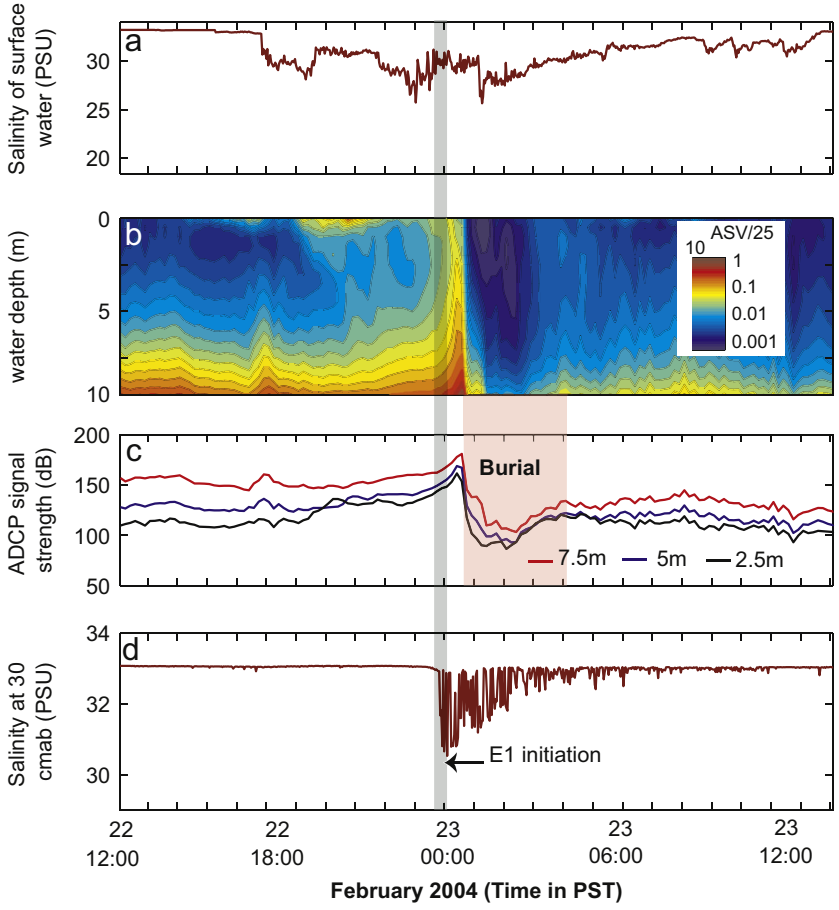

Fig. 14. Apparent burial of the TRBM-mounted ADCP as shown by reductions in the acoustic scattering volume (ASV in dB) and raw ADCP signal strength 1 h after the initiation of the E1 event.

of the river sediment flux is predicted to enter into the observed sediment gravity current. The sediment flux during E2 was surely greater than during E1, but it could not be estimated due to the incomplete records of this event.

4.4. Sediment settling rates

The presence of a hyperpycnal gravity current at such close proximity to the river mouth begs the question of how

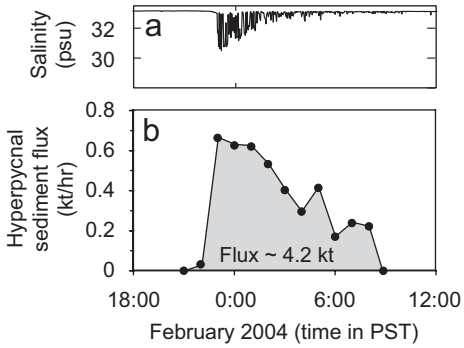

Fig. 15. Comparison of the estimated offshore sediment flux in the gravity current with the salinity observations at 30 cmab during event E1. The total estimated sediment flux during the 11-h event is 4.2 kt.

this sediment got to the seabed and became such an event. From observations and modeling it is clear that such events only occur when fine-grained sediment loading to the seabed overweighs the transport potential of the wave-current-suspended sediment (Harris et al., 2005). We thus look to a simple sediment supply model to evaluate sediment supply and settling processes.

For this model, we assume that the water column offshore of the river mouth consists of three layers, the buoyant plume, the ambient water, and the gravity current, each with representative across-shore velocities (u_{plume}, $u_{current}$, and u_g; Fig. 16(a)). The sediment is then placed at the river mouth and given a constant settling velocity w_s based on the settling process: individual grain (0.1 mm/s), flocs (1 mm/s), or convective instabilities (20 mm/s). The plume thickness is based on CTD results at ~1 km from the river mouth presented in Warrick et al. (2004a), and assumed to be a constant 3 m with the model domain (Fig. 16(a)). Acoustic observations were used to assess the current speeds: u_{plume} were measured to be ~20 cm/s by the ADCP during both E1 and E2, although Warrick et al. (2004b, 2007) report that across-shore currents off the Santa Clara River mouth can exceed 50 cm/s, thus we used a range of 20–50 cm/s; $u_{current}$ were measured to be 0–10 cm/s throughout the water column, commonly highest near the surface and approaching zero near the seabed, during both E1 and E2 with a mean of 5 cm/s (cf. Fig. 5); u_g was ~5 cm/s as noted above.

Individual grain settling would transport the sediment many kilometers offshore before settling from the buoyant plume (Fig. 16(b)). Flocs on the other hand settle quickly from the buoyant plume, although this settling process would deliver sediment beyond the extent of the moorings (Fig. 16(b)). Further, we note that the minimum total settling time of flocs is 3 h, which approximately coincides with the beginning of the gravity currents. An enhanced settling process such as convective instabilities (cf. McCool and Parsons, 2004) would deliver the sediment to the seabed within 200 m of the river mouth (Fig. 16(b)), and this would take a maximum of only 10 min to place the

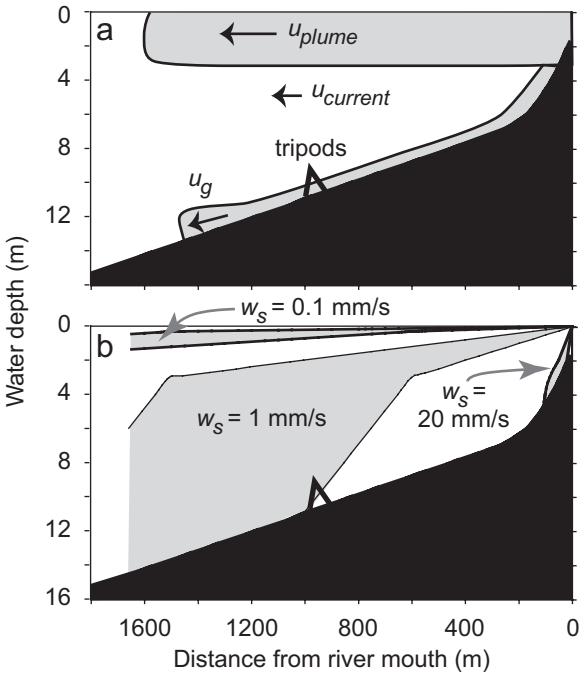

Fig. 16. Sediment settling model for across-shore dispersal from the Santa Clara River. (a) Model framework with cross-shore velocities (u) labeled. (b) Results of the model with three types of sediment settling, individual grains, flocs and convective instabilities, and their respective settling velocities (w_s = 0.1, 1, and 20 mm/s). Shaded region represents the bounds of particle trajectories based on parameters detailed in the text.

sediment on the seabed. Once on the bed, this sediment would travel downslope at u_g, which would take 4–5 h to reach the tripods—values remarkably close to the 4–6 h lag time observed. This simplified model suggests that the gravity current may have formed within hundreds of meters of the river mouth, thus requiring a process of rapid sediment settling.

4.5. Dispersal conceptual model

The combined measurements presented here have been integrated into a hypothetical dispersal model for river discharge events (Fig. 17) based on the findings and assumptions above. Coincidental to the formation of a buoyant plume, a significant portion (~25–50% for the events observed here) of the discharged sediment rapidly settles to the seafloor and forms a hyperpycnal plume that is transported offshore due to gravitational forcing and wave resuspension (Fig. 17(a) and (b)). This sediment transport occurs within tens of centimeters of the seabed, is formed within 1 km of the river mouth, and likely results from enhanced effective settling rates from convective instabilities, negative buoyancy, or perhaps other downward mixing processes (cf. Mulder and Syvitski, 1995; McCool and Parsons, 2004; Milligan et al., 2007). Transport of this sediment offshore to the mid-shelf is dictated by wave-dependent gravity-driven sediment transport, since the shelf slope becomes very flat (0.005) offshore

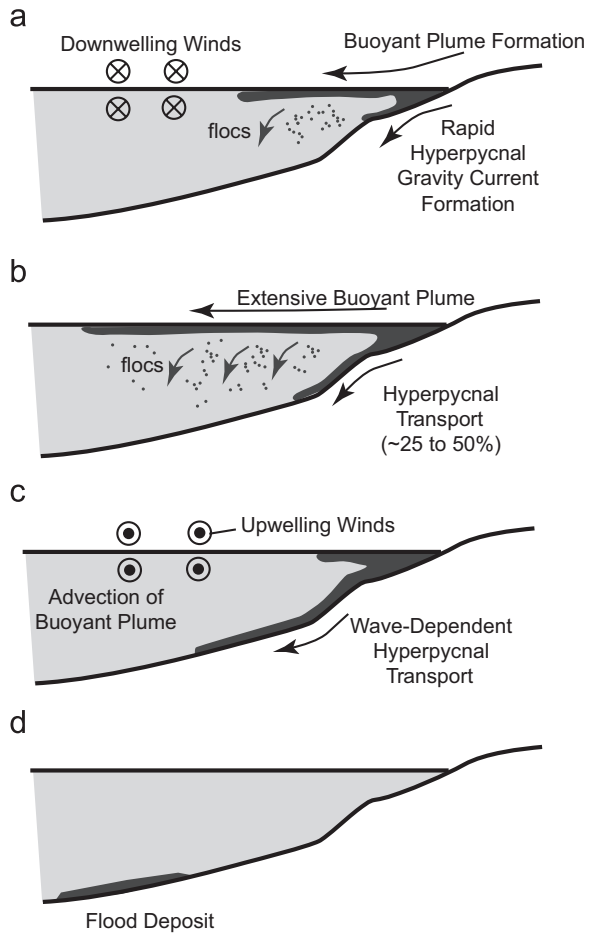

Fig. 17. Conceptual model summarizing dispersal of fine-grained sediment from the Santa Clara River onto the Ventura Shelf. (a) Event Initiation; (b) Peak River Discharge; (c) Post-Event Dynamics and (d) Flood Sedimentation.

of the river mouth (Fig. 17(c); cf. Wright et al., 2001). Orbital velocities from large wave events, such as those observed on February 26 (Fig. 4), are likely to provide an important mechanism for transporting this sediment to the mid-shelf, where event and long-term fine-grained sediment accumulates (Drake et al., 1972). It is likely that floc formation and settling (cf. Geyer et al., 2000; Hill et al., 2007) are also important processes for delivering fine-grained sediment to the seabed (Fig. 17(b)), because: (1) the gravity currents observed herein could not account for more than about half of the discharged sediment, and (2) settling of sediment from the buoyant plume continues at rates that suggest floc formation (cf. Warrick et al., 2004a).

5. Conclusions

The observations of the hyperpycnal plumes shown here are unique because they show a very rapid formation of these conditions on a sand-dominated portion of the inner shelf offshore of a small, mountainous river. This sediment transport mechanism appeared to be a major sediment pathway during the events observed, and we note that the fate of this sediment might be very different than sediment delivered to the seabed over longer periods of time by slower settling rates. Once on the seabed, sediment transport direction in the hyperpycnal current will be directed downslope, i.e., "steered" by topography, whereas sediment still suspended throughout the water column will be subject to advection by currents. As noted by Geyer et al. (2000) these currents can spread sediment many to tens of kilometers away from the river mouth even when the sediment is packaged in flocs. Thus, sediment transported in events like those observed here may be deposited in very different locations than that expected by sediment transport models based on other observations. An example of river mouth where this topographic influence is significant is the Sepik River margin, where a canyon intercepts gravity-current transport and the shelf receives much of the sediment suspended in the buoyant plume (Kineke et al., 2000). Hyperpycnal pathways from the Santa Clara River will likely be more important for events larger than those observed here, which not only discharge at higher suspended-sediment concentrations, but also dominate the long-term sediment budget (Warrick and Milliman, 2003).

Future investigation may reveal that rapid formation of hyperpycnal sediment plumes occurs offshore of many other river systems, especially those that discharge sediment at concentrations of many to tens of g/l. Many remaining questions exist, including: how does sediment rapidly settle and/or mix to the seabed under such conditions (cf. McCool and Parsons, 2004); what are the grain-size and geochemical characteristics of sediment in these transport events; and how do these events influence marine sediment budgets? The work presented here has offered evidence that these events occur somewhat frequently (1–3 year recurrence) and are an important element of the sediment mass balance for a river such as the Santa Clara. Future work may reveal further details of the formation, nature, and impact of these events.

Acknowledgments

These observations were made possible by funding from the USGS Mendenhall Postdoctoral Research Fellowship Program and the USGS Coastal and Marine Geology Program. We would like to thank Joanne Thede Ferreira, Dave Gonzales, Hal Williams, the crews of the R/V *Seawatch* and R/V *Yellowfin*, and the staff from Divecon for assistance with instrument calibration, deployment, and recovery. Kurt Rosenberger assisted with data analyses, and Patrick Barnard collected and provided Santa Clara River mouth bathymetry data. An earlier version of the manuscript was improved by the comments of Dan Hanes and Curt Storlazzi. Carl Friedrichs and an anonymous reviewer provided helpful reviews on this final edition of the paper.

References

Ahn, J.H., Grant, S.B., Surbeck, C.Q., DiGiacomo, P.M., Nezlin, N.N., Jiang, S., 2005. Coastal water quality impact of storm water runoff from an urban watershed in southern California. Environmental Science and Technology 39, 5940–5953.

Archie, G.E., 1942. Electrical resistivity log as an aid in determining some reservoir characteristics. Journal of Petroleum Technology 5, 1–8.

Berner, R.A., 1982. Burial of organic carbon and pyrite sulfur in the modern ocean: its geochemical and environmental significance. American Journal of Science 282, 451–473.

California Department of Water Resources (CADWR), 2007. Online CADWR Division of Flood Management records for the OJA station in Ojai. 〈http://cdec.water.ca.gov/〉 (accessed July 20, 2007).

Cerda, A., 1998. Post-fire dynamics of erosional processes under Mediterranean climatic conditions. Zeitschrift fuer Geomorphologie 42 (3), 373–398.

Conner, C.S., DeVisser, A.M., 1992. A laboratory investigation of particle size effects on an optical backscatterance sensor. Marine Geology 108, 151–159.

Drake, D.E., Kolpack, R.L., Fischer, P.J., 1972. Sediment transport on the Santa Barbara-Oxnard Shelf, Santa Barbara Channel, California. In: Swift, D.J.P., Duane, D.B., Pilkey, O.H. (Eds.), Shelf Sediment Transport: Process and Pattern. Dowden, Hutchinson & Ross, Inc., Stroudsburg, PA (Chapter 14).

Dojiri, M., Yamaguchi, M., Weisberg, S.B., Lee, H.J., 2003. Changing anthropogenic influence on the Santa Monica Bay watershed. Marine Environmental Research 56, 1–14.

Florsheim, J.L., Keller, E.A., Best, D.W., 1991. Fluvial sediment transport in response to moderate storm flows following chaparral wildfire, Ventura County, southern California. Geological Society of America Bulletin 103 (4), 504–511.

Fredsøe, J., Deigaard, R., 1992. Mechanics of Coastal Sediment Transport. World Scientific, New Jersey, 369pp.

Garvine, R.W., 1974. Physical features of the Connecticut River outflow during high discharge. Journal of Geophysical Research 79 (6), 831–846.

George, D.A., Hill, P.S., Milligan, T.G., 2007. Flocculation, heavy metals (Cu, Pb, Zn) and the sand–mud transition on the Adriatic continental shelf, Italy. Continental Shelf Research 27 (3-4), 475–488.

Geyer, W.R., Hill, P., Milligan, T., Traykovski, P., 2000. The structure of the Eel River plume during floods. Continental Shelf Research 20, 2067–2093.

Gibbs, R.J., Wolanski, E., 1992. The effect of flocs on optical backscattering measurements of suspended material concentration. Marine Geology 107 (4), 289–291.

Gordon, E.S., Goñi, M.A., 2004. Controls on the distribution and accumulation of terrigenous organic matter in sediments from the Mississippi and Atchafalaya River margin. Marine Chemistry 92, 331–352.

Hamilton, E.L., 1972. Compressional-wave attenuation in marine sediments. Geophysics 37 (4), 620–646.

Harris, C.K., Traykovski, P.A., Geyer, W.R., 2005. Flood dispersal and deposition by near-bed gravitational sediment flows and oceanographic transport: a numerical modeling study of the Eel River shelf, northern California. Journal of Geophysical Research 110, C09025.

Hedges, J.I., Keil, R.G., 1995. Sedimentary organic matter preservation: an assessment and speculative synthesis. Marine Chemistry 49, 81–115.

Hill, P.S., Milligan, T.G., Geyer, W.R., 2000. Controls on effective settling velocity of suspended sediment in the Eel River flood plume. Continental Shelf Research 20 (16), 2095–2111.

Hill, P.S., et al., 2007. Sediment delivery to the seabed on continental margins. In: Nittrouer, C.A., et al. (Eds.), Continental Margin Sedimentation: From Sediment Transport to Sequence Stratigraphy. Special Publication Number 37, International Association of Sedimentologists.

Hoitink, A.J.F., Hoekstra, P., 2005. Observations of suspended sediment from ADCP and OBS measurements in a mud-dominated environment. Coastal Engineering 52, 103–118.

Hutchins, D.A., DiTullio, G.R., Zhang, Y., Bruland, K.W., 1998. An iron limitation mosaic in the California upwelling regime. Limnology and Oceanography 43 (6), 1037–1054.

Jackson, P.D., Taylor-Smith, D., Stanford, P.N., 1978. Resistivity–porosity–particle shape relationships for marine sands. Geophysics 43, 1250–1268.

Johnson, K.S., Chavez, F.P., Friederich, G.E., 1999. Continental-shelf sediment as a primary source of iron for coastal phytoplankton. Nature 398, 697–700.

Kineke, G.C., Sternberg, R.W., 1992. Measurements of high concentration suspended sediments using the optical backscatterance sensor. Marine Geology 108, 253–258.

Kineke, G.C., Sternberg, R.W., Trowbridge, J.H., Geyer, W.R., 1996. Fluid mud processes on the Amazon continental shelf. Continental Shelf Research 16, 667–696.

Kineke, G., Woolfe, K.J., Kuehl, S.A., Milliman, J., Dellapena, T., Purdon, R.G., 2000. Sediment export from the Sepik River, Papua New Guinea: evidence for a divergent dispersal system. Continental Shelf Research 20, 2239–2266.

Lave, J., Burbank, D., 2004. Denudation processes and rates in the Tranverse Ranges, southern California: erosional response of a transitional landscape to external and anthropogenic forcing. Journal of Geophysical Research 109, F01006.

Lee, G., Friedrichs, C.T., Vincent, C.E., 2002. Examination of diffusion versus advection dominated sediment suspension on the inner shelf under storm and swell conditions, Duck, North Carolina. Journal of Geophysical Research 107 (C7), 3084.

Los Angeles County Flood Control District (LACFCD), 1959. Report on debris reduction studies for mountainous watersheds of Los Angeles County. Los Angeles, CA, 164pp.

Ludwig, K.A., Hanes, D.M., 1990. A laboratory evaluation of optical backscatterance suspended solids sensors exposed to sand–mud mixtures. Marine Geology 94, 173–179.

Lynch, J.F., Irish, J.D., Sherwood, C.R., Agrawal, Y.C., 1994. Determining suspended sediment particle size information from acoustical and optical backscatter measurements. Continental Shelf Research 14 (10/11), 1139–1165.

McCool, W.W., Parsons, J.D., 2004. Sedimentation from buoyant fine-grained suspensions. Continental Shelf Research 24, 1129–1142.

Mertes, L.A.K., Warrick, J.A., 2001. Measuring flood output from 110 coastal watersheds in California with field measurements and SeaWIFS. Geology 29, 659–662.

Milligan, T.G., Hill, P.S., Law, B.A., 2007. Flocculation and the loss of sediment from the Po River plume. Continental Shelf Research 27, 309–321.

Milliman, J.D., Syvitski, J.P.M., 1992. Geomorphic/tectonic control of sediment discharge to the ocean: the importance of small mountainous rivers. Journal of Geology 100, 525–544.

Mulder, T., Syvitski, J.P.M., 1995. Turbidity currents generated at river mouths during exceptional discharge to the world oceans. Journal of Geology 103, 285–298.

Nash, J.D., Moum, J.N., 2005. River plumes as a source of large-amplitude internal waves in the coastal ocean. Nature 437 (7057), 400–403.

Parsons, J.D., Bush, J.W.M., Syvitski, J.P.M., 2001. Hyperpycnal plume formation from riverine outflows with small sediment concentrations. Sedimentology 48 (2), 465–478.

Parsons, J.D., et al., 2007. The mechanics of marine sediment gravity flows. In: Nittrouer, C.A., et al. (Eds.), Continental Margin Sedimentation: From Sediment Transport to Sequence Stratigraphy. Special Publication Number 37, International Association of Sedimentologists.

Rice, R.M., 1982. Sedimentation in the chaparral: how do you handle unusual events? In: Swanson, F.J., Janda, R.J., Dunne, T., Swanston, D.N. (Eds.), Sediment budgets and routing in forested drainage basins. General Technical Report PNW-141, Pacific Northwest Forest and Range Experiment Station.

Scully, M.E., Friedrichs, C.T., Wright, L.D., 2003. Numerical modeling of gravity-driven sediment transport and deposition on an energetic continental shelf: Eel River, northern California. Journal of Geophysical Research 108 (C4), 3120.

Sherwood, C.R., Lacy, J.R., Voulgaris, G., 2006. Shear velocity estimates on the inner shelf off Grays Harbor, Washington, USA. Continental Shelf Research 26, 1995–2018.

Smith, J.D., Mclean, J.R., 1977. Spatially averaged flow over a wavy surface. Journal of Geophysical Research 82, 1735–1746.

Syvitski, J.P.M., Vörösmarty, C.J., Kettner, A.J., Green, P., 2005. Impact of humans on the flux of terrestrial sediment to the global coastal ocean. Science 308, 376–380.

Taylor, B.D., 1981. Inland sediment movements by natural processes. In: Sediment management for southern California mountains, coastal plains and shoreline. Environmental Quality Laboratory Report No. 17-B, California Institute of Technology, Pasadena (Part B).

Thorne, P.D., Hardcastle, P.J., Soulsby, R.L., 1993. Analysis of acoustic measurements of suspended sediments. Journal of Geophysical Research 98 (C1), 899–910.

Traykovski, P., Geyer, W.R., Irish, J.D., Lynch, J.F., 2000. The role of wave-induced density-driven fluid mud flows for cross-shelf transport on the Eel River continental shelf. Continental Shelf Research 20, 2113–2140.

Traykovski, P., Wiberg, P.L., Geyer, W.R., 2007. Observations and modeling of wave-supported sediment gravity flows on the Po prodelta and comparison to prior observations from the Eel shelf. Continental Shelf Research 27, 375–399.

Trowbridge, J.H., Kineke, G.C., 1994. Structure and dynamics of fluid muds over the Amazon continental shelf. Journal of Geophysical Research 99, 865–874.

Warrick, J.A., 2002. Short-term (1997–2000) and long-term (1928–2000) observations of river water and sediment discharge to the Santa Barbara Channel, California. Ph.D. Dissertation, University of California, Santa Barbara. 337pp.

Warrick, J.A., Milliman, J.D., 2003. Hyperpycnal sediment discharge from semiarid southern California rivers: implications for coastal sediment budgets. Geology 31, 781–784.

Warrick, J.A., Mertes, L.A.K., Washburn, L., Siegel, D.A., 2004a. A conceptual model for river water and sediment dispersal in the Santa Barbara Channel, California. Continental Shelf Research 24, 2029–2043.

Warrick, J.A., Mertes, L.A.K., Washburn, L., Siegel, D.A., 2004b. Dispersal forcing of a southern California river plume, based on field and remote sensing observations. Geo-Marine Letters 24 (1), 46–52.

Warrick, J.A., Rubin, D.M., 2007. Suspended-sediment rating curve response to urbanization and wildfire, Santa Ana River, California. Journal of Geophysical Research 112, F02018.

Warrick, J.A., DiGiacomo, P.M., Weisberg, S.B., Nezlin, N.P., Mengel, M., Jones, B.H., Ohlmann, J.C., Washburn, L., Terrill, E.J., Farnsworth, K.L., 2007. River plume patterns and dynamics within the Southern California Bight. Continental Shelf Research 27, 2427–2448.

Wiberg, P., Smith, J.D., 1983. A comparison of field data and theoretical models for wave–current interactions at the bed on the continental shelf. Continental Shelf Research 2 (2–3), 147–162.

Wolanski, E., Richmond, R.H., Davis, G., Bonito, V., 2003. Water and fine sediment dynamics in transient river plumes in a small, reef-fringed bay, Guam. Estuarine, Coastal and Shelf Science 56 (5–6), 1029–1040.

Wright, L.D., Nittrouer, C.A., 1995. Dispersal of river sediments in coastal seas: six contrasting cases. Estuaries 18, 494–508.

Wright, L.D., Friedrichs, C.T., Kim, S.C., Scully, M.E., 2001. Effects of ambient currents and waves on gravity-driven sediment transport on continental shelves. Marine Geology 175, 25–45.

Wright, L.D., Friedrichs, C.T., Scully, M.E., 2002. Pulsational gravity-driven sediment transport on two energetic shelves. Continental Shelf Research 22, 2443–2460.

Wright, L.D., Friedrichs, C.T., 2006. Gravity-driven sediment transport on continental shelves: a status report. Continental Shelf Research 26 (17–18), 2092–2107.